Research Article | Vol. 25, No. 16 | 7 Aug 2017 | OPTICS EXPRESS 18537

Optics EXPRESS

Organic membrane photonic integrated circuits (OMPICs)

TOMOHIRO AMEMIYA,[1,2,*] TORU KANAZAWA,[1] TAKUO HIRATANI,[1] DAISUKE INOUE,[1] ZHICHEN GU,[1] SATOSHI YAMASAKI,[1] TATSUHIRO URAKAMI,[3] AND SHIGEHISA ARAI[1,2,4]

[1]*Institute of Innovative Research (IIR), Tokyo Institute of Technology, 2-12-1 O-okayama, Meguro-ku, Tokyo 152-8552, Japan*
[2]*Department of Electrical and Electronic Engineering, Tokyo Institute of Technology, 2-12-1 O-okayama, Meguro-ku, Tokyo 152-8552, Japan*
[3]*Functional Materials Laboratory, Mitsui Chemicals, Inc., Chiba 299-0265, Japan*
[4]*arai@pe.titech.ac.jp*
[*]*amemiya.t.ab@m.titech.ac.jp*

Abstract: We propose the concept of organic membrane photonic integrated circuits (OMPICs), which incorporate various functions needed for optical signal processing into a flexible organic membrane. We describe the structure of several devices used within the proposed OMPICs (e.g., transmission lines, I/O couplers, phase shifters, photodetectors, modulators), and theoretically investigate their characteristics. We then present a method of fabricating the photonic devices monolithically in an organic membrane and demonstrate the operation of transmission lines and I/O couplers, the most basic elements of OMPICs.

OCIS codes: (130.0130) Integrated optics; (310.6845) Thin film devices and applications; (160.5470) Polymers.

References and links

1. S. E. Miller, "Integrated Optics: An Introduction," Bell Labs Tech. J. **48**(7), 2059–2069 (1969).
2. E. A. J. Marcatili, "Dielectric rectangular waveguide and directional coupler for integrated optics," Bell Labs Tech. J. **48**(7), 2071–2102 (1969).
3. Y. Suematsu, "Integrated Optics," Convention Record Four Institutes Electrical Eng. **1223**, 430 (1971).
4. L. A. Coldren, S. C. Nicholes, L. Johansson, S. Ristic, R. S. Guzzon, E. J. Norberg, and U. Krishnamachari, "High performance InP-based photonic ICs—A tutorial," J. Lightwave Technol. **29**(4), 554–570 (2011).
5. R. Nagarajan, M. Kato, D. Lambert, P. Evans, S. Corzine, V. Lal, J. Rahn, A. Nilsson, M. Fisher, M. Kuntz, J. Pleumeekers, A. Dentai, H.-S. Tsai, D. Krause, H. Sun, K.-T. Wu, M. Ziari, T. Butrie, M. Reffle, M. Mitchell, F. Kish, and D. Welch, "Terabit/s class InP photonic integrated circuits," Semicond. Sci. Technol. **27**(9), 094003 (2012).
6. J. K. Doylend and A. P. Knights, "The evolution of silicon photonics as an enabling technology for optical interconnection," Laser Photonics Rev. **6**(4), 504–525 (2012).
7. P. P. Absil, P. Verheyen, P. De Heyn, M. Pantouvaki, G. Lepage, J. De Coster, and J. Van Campenhout, "Silicon photonics integrated circuits: a manufacturing platform for high density, low power optical I/O's," Opt. Express **23**(7), 9369–9378 (2015).
8. M. J. R. Heck, H.-W. Chen, A. W. Fang, B. R. Koch, D. Liang, H. Park, M. Sysak, and J. E. Bowers, "Hybrid silicon photonics for optical interconnects," IEEE J. Sel. Top. Quantum Electron. **17**(2), 333–346 (2011).
9. Z. Zhou, B. Yin, and J. Michel, "On-chip light sources for silicon photonics," Light Sci. Appl. **4**(11), e358 (2015).
10. D.-H. Kim, J.-H. Ahn, W. M. Choi, H.-S. Kim, T.-H. Kim, J. Song, Y. Y. Huang, Z. Liu, C. Lu, and J. A. Rogers, "Stretchable and Foldable Silicon Integrated Circuits," Science **320**(5875), 507–511 (2008).
11. J. Lee, J. Wu, M. Shi, J. Yoon, S. I. Park, M. Li, Z. Liu, Y. Huang, and J. A. Rogers, "Stretchable GaAs Photovoltaics with Designs That Enable High Areal Coverage," Adv. Mater. **23**(8), 986–991 (2011).
12. M. Kaltenbrunner, T. Sekitani, J. Reeder, T. Yokota, K. Kuribara, T. Tokuhara, M. Drack, R. Schwödiauer, I. Graz, S. Bauer-Gogonea, S. Bauer, and T. Someya, "An ultra-lightweight design for imperceptible plastic electronics," Nature **499**(7459), 458–463 (2013).
13. R. T. Chen, "Polymer-based photonic integrated circuits," Opt. Laser Technol. **25**(6), 347–365 (1993).
14. L. Eldada and L. W. Shacklette, "Advances in polymer integrated optics," IEEE J. Quantum Electron. **6**(1), 54–68 (2000).
15. Z. Zhang, D. Felipe, V. Katopodis, P. Groumas, C. Kouloumentas, H. Avramopoulos, J.-Y. Dupuy, A. Konczykowska, A. Dede, A. Beretta, A. Vannucci, G. Cangini, R. Dinu, D. Schmidt, M. Moehrle, P. Runge, J.-

#296552 https://doi.org/10.1364/OE.25.018537
Journal © 2017 Received 23 May 2017; revised 18 Jul 2017; accepted 18 Jul 2017; published 24 Jul 2017

Optics EXPRESS

H. Choi, H.-G. Bach, N. Grote, N. Keil, and M. Schell, "Hybrid photonic integration on a polymer platform," Photonics **2**(3), 1005–1026 (2015).
16. L. Li, H. Lin, S. Qiao, Y. Zou, S. Danto, K. Richardson, J. D. Musgraves, N. Lu, and J. Hu, "Integrated flexible chalcogenide glass photonic devices," Nat. Photonics **8**(8), 643–649 (2014).
17. T. Amemiya, T. Kanazawa, and S. Arai, "Organic membrane photonic integrated circuits," PCT application No. PCT/JP2017/012136.
18. R. Yoshimura, M. Hikita, S. Tomaru, and S. Imamura, "Low-loss polymeric optical waveguides fabricated with deuterated polyfluoromethacrylate," J. Lightwave Technol. **16**(6), 1030–1037 (1998).
19. T. Watanabe, N. Ooba, S. Hayashida, T. Kurihara, and S. Imamura, "Polymeric optical waveguide circuits formed using silicone resin," J. Lightwave Technol. **16**(6), 1049–1055 (1998).
20. Q. Bao and K. P. Loh, "Graphene photonics, plasmonics, and broadband optoelectronic devices," ACS Nano **6**(5), 3677–3694 (2012).
21. F. Xia, H. Wang, D. Xiao, M. Dubey, and A. Ramasubramaniam, "Two-dimensional material nanophotonics," Nat. Photonics **8**(12), 899–907 (2014).
22. T. Kanazawa, T. Amemiya, A. Ishikawa, V. Upadhyaya, K. Tsuruta, T. Tanaka, and Y. Miyamoto, "Few-layer HfS2 Transistors," Sci. Rep. **6**(1), 22277 (2016).
23. M. Chhowalla, D. Jena, and H. Zhang, "Two-dimensional semiconductors for transistors," Nat. Rev. Mater. **1**(11), 16052 (2016).
24. S. H. Mousavi, I. Kholmanov, K. B. Alici, D. Purtseladze, N. Arju, K. Tatar, D. Y. Fozdar, J. W. Suk, Y. Hao, A. B. Khanikaev, R. S. Ruoff, and G. Shvets, "Inductive tuning of Fano-resonant metasurfaces using plasmonic response of graphene in the mid-infrared," Nano Lett. **13**(3), 1111–1117 (2013).
25. M. S. Kwon, "Discussion of the epsilon-near-zero effect of graphene in a horizontal slot waveguide," IEEE Photonics J. **6**(3), 1–9 (2014).
26. A. Y. Nikitin, F. J. Garcia-Vidal, and L. Martin-Moreno, "Analytical expressions for the electromagnetic dyadic Green's function in graphene and thin layers," IEEE J. Sel. Top. Quantum Electron. **19**(3), 4600611 (2013).
27. E. H. Hwang and S. D. Sarma, "Single-particle relaxation time versus transport scattering time in a two-dimensional graphene layer," Phys. Rev. B **77**(19), 195412 (2008).
28. K. Fukukawa, M. Okazaki, Y. Sakata, T. Urakami, and A. Okubo, "Transparent Polyimide and Precursor Thereof," PCT application No. PCT/JP2014/062474.
29. T. Okamoto, N. Nunoya, Y. Onodera, S. Tamura, and S. Arai, "Continuous wave operation of optically pumped membrane DFB laser," Electron. Lett. **37**(24), 1455 (2001).
30. S. Arai, N. Nishiyama, T. Maruyama, and T. Okumura, "GaInAsP/InP membrane lasers for optical interconnects," IEEE J. Sel. Top. Quantum Electron. **17**(5), 1381–1389 (2011).
31. D. Inoue, J. Lee, T. Hiratani, Y. Atsuji, T. Amemiya, N. Nishiyama, and S. Arai, "Sub-milliampere threshold operation of butt-jointed built-in membrane DFB laser bonded on Si substrate," Opt. Express **23**(6), 7771–7778 (2015).
32. V. Dolores-Calzadilla, D. Heiss, and M. Smit, "Highly efficient metal grating coupler for membrane-based integrated photonics," Opt. Lett. **39**(9), 2786–2789 (2014).
33. G. Beadie, M. Brindza, R. A. Flynn, A. Rosenberg, and J. S. Shirk, "Refractive index measurements of poly(methyl methacrylate) (PMMA) from 0.4-1.6 μm," Appl. Opt. **54**(31), F139–F143 (2015).
34. http://www.agcce.com/cytop-technical-information/
35. J. Halldorsson, N. B. Arnfinnsdottir, A. B. Jonsdottir, B. Agnarsson, and K. Leosson, "High index contrast polymer waveguide platform for integrated biophotonics," Opt. Express **18**(15), 16217–16226 (2010).

1. Introduction: organic-membrane platform opens new fields of photonic ICs

This paper proposes a flexible (bendable) photonic integrated circuit that is constructed in an organic membrane. This device is capable of being bent and twisted without breaking, and is expected to open new fields of application for photonic systems.

A photonic integrated circuit (PIC) is a device that incorporates the multiple photonic functions needed for optical communication and processing on a single chip. PICs have many advantages over their discrete counterparts, such as their small size, low cost, high reliability, and low power consumption. Therefore, various PICs have been developed, and these now dominate the market for optical systems and components.

The history of PICs began in 1969, when Bell Laboratories introduced the concept of integrated optics in a special issue of the Bell System Technical Journal [1]. Most technological concepts essential to PICs, including the propagation-mode analysis formalized by Miller [1] and Marcatili [2], were established at this time. Two years later, Suematsu advanced the concept of PICs to the current level by proposing the integration of semiconductor lasers, optical parametric oscillators, wavelength multiplexers, and other sophisticated photonic functions [3].

Optics EXPRESS

Currently, the most widely used commercial platform material for PICs is InP [4, 5]. This is because the InP platform enables the monolithic integration of light sources (or lasers) with other optical and electronic elements, which is very convenient when making PICs for fiber-optic communication. However, if an external light source is allowable, silicon-on-insulator (SOI) is a superior PIC platform because it provides low-loss waveguides and high-density integration. Many institutions have started to research and develop silicon PICs in an attempt to attain low-cost, high-performance photonic circuits [6, 7]. Although the light source is a weak point of silicon PICs, advances in wafer bonding techniques mean that the hybrid integration of III-V semiconductor lasers into silicon PICs will soon be a practical solution [8, 9]. As this wave of material innovation comes to PICs, the market for InP-based PICs is likely to decrease significantly.

As part of this innovative advance, we focus on an organic membrane as a new platform material for PICs. Organic films have recently been introduced into the field of electronic devices, creating various new application fields that were impossible with conventional semiconductor devices [10–12]. Similar developments can be expected for photonic devices. The use of organic membranes instead of conventional rigid platforms (GaAs, InP, Si, and glass) will provide flexible, lightweight, wearable, and large-area PIC devices for sensing, monitoring, and data processing in various security, biomedical, and healthcare applications.

Several studies on optical transmission technology have been conducted using organic materials [13–15]. However, most research has used only simple passive devices such as optical waveguides and transmission lines. This is because it is more difficult to assign electronic functionalities to organic materials than to InP and Si. Recently, more sophisticated device elements such as ring resonators have been made using organic materials [16], but these remain at the experimental level. Organic PICs are still far from their InP and Si counterparts in terms of integration and functionality.

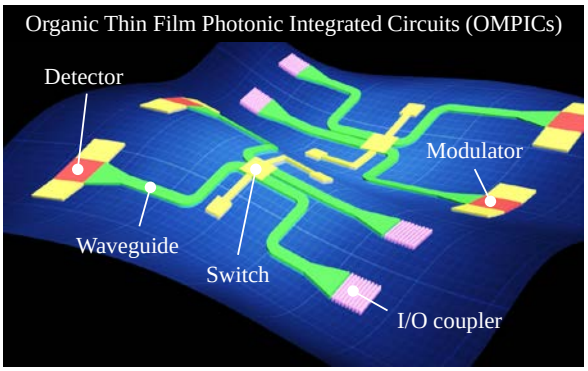

Fig. 1. Conceptual diagram of OMPIC (organic membrane photonic integrated circuit).

In this paper, we propose a structure of organic PICs that can incorporate various functions (except a light source) needed for optical signal processing into a flexible organic membrane [17]. We hereafter refer to this PIC structure as the OMPIC (organic membrane photonic integrated circuit); its conceptual diagram is shown in Fig. 1. To realize a working OMPIC, it is necessary to give electronic functionality to organic films. For this purpose, we first propose a method of incorporating functional materials into an organic membrane (Section 2). Then, we propose an example of a fabrication process that integrates various photonic devices monolithically in a membrane (Section 3). The characteristics of the devices given by this process are estimated using theoretical calculations (Section 4). As the first step in actual device fabrication, we construct transmission lines and I/O couplers that are monolithically integrated in an organic membrane. Their operation is demonstrated in Section 5.

Optics EXPRESS

2. Incorporating functional materials into organic membranes

Organic polymers are suitable materials for flexible, lightweight, and low-cost optical fibers required in short-range transmission systems such as in-device, in-building, and in-car networks. Various polymers have been synthesized for a wide range of optical, mechanical and thermal requirements [18, 19]. As a material for PICs, however, they have a problem—their electronic functionality is much worse than that of InP and Si. To overcome this problem and construct effective OMPICs, we propose a technique for incorporating electronic materials into an organic membrane. The material for this purpose must meet the following requirements:

(i) It must exhibit a photo-induced change in, for example, carrier concentration, conductivity, refractive index, and transmittance in response to light from the optical communication band to the visible band.

(ii) It must be flexible. That is, it should be capable of being bent and twisted without breaking.

In the following, we present two candidate materials and describe their incorporation into an organic membrane. Fabricated samples are also presented.

2.1 Graphene

Graphene is a two-dimensional material consisting of a single layer of carbon atoms bonded together in a hexagonal honeycomb lattice; this structure offers excellent flexibility because of its strong carbon–carbon bonds. The Dirac-cone band structure of graphene results in unique optical and electrical properties, such as a very large carrier mobility and conductivity, despite the structure being extremely thin. The chemical potential of graphene can be changed over a wide range with an electric field applied perpendicular to the surface of the graphene, and consequently the optical and electrical behavior change drastically. Many studies have used graphene for optical and electrical devices [20–23].

Graphene can be treated as an uniaxial medium with a dielectric tensor having an effective surface-normal component $\varepsilon_0\varepsilon_{yy}$ and effective in-plane components $\varepsilon_0\varepsilon_{xx}$ and $\varepsilon_0\varepsilon_{zz}$ [24, 25]. The value of ε_{yy} is 1, and ε_{xx} and ε_{zz} are given by

$$\varepsilon = 1 + \frac{i\sigma_g}{\omega\varepsilon_0 d_g} \tag{1}$$

where σ_g and d_g (= 0.35 nm) are the optical conductivity and the effective thickness of graphene, ω is the angular frequency of light, and ε_0 is the vacuum permittivity. Within the random-phase approximation, the optical conductivity of graphene can be derived from the Kubo formula in a complex form consisting of interband and intraband contributions [26]. It is expressed by

$$\begin{aligned}\sigma_g = \frac{e^2}{4\hbar}\left(\frac{1}{2} + \frac{1}{\pi}\arctan\left(\frac{\hbar\omega - 2|\mu|}{2k_BT}\right) - \frac{i}{2\pi}\ln\frac{\left(\hbar\omega + 2|\mu|\right)^2}{\left(\hbar\omega - 2|\mu|\right)^2 + \left(2k_BT\right)^2}\right) \\ + \frac{2ie^2k_BT}{\hbar^2\pi\left(\omega + i\tau^{-1}\right)}\ln\left(2\cosh\left(\frac{|\mu|}{2k_BT}\right)\right)\end{aligned} \tag{2}$$

where $\hbar$ is the reduced Planck constant, k_B Boltzmann constant, T temperature, and τ the relaxation time in graphene. In the calculation, T and τ were set to 300 K and 0.1 ps [27].

The effects of inter- and intra-band transition on graphene conductivity depend on chemical potential μ of the graphene and frequency ω of incident light. The chemical potential is a function of carrier concentration, and therefore the optical properties of

Optics EXPRESS

graphene for a given light frequency can be changed by controlling the carrier concentration with impurity doping and electrical gating. If $|\mu|>\hbar\omega/2$, intraband transition is dominant, and graphene shows metalic behavior. If $|\mu|<\hbar\omega/2$, interband transition occurs, and dielectric behavior appears.

Figure 2 shows the in-plane refractive index *n* and extinction coefficient *k* of graphene as a function of the chemical potential calculated using Eqs. (1)–(2) for the optical communication frequency (wavelength = 1550 nm). The optical behavior of graphene strongly depends on the chemical potential μ; it is dielectric-like at 0 eV < μ < 0.4 eV because of interband absorption and metallic at μ > 0.5 eV because of intraband absorption. This can be used to develop photonic functions, as described in Section 4.

When incorporating graphene into OMPICs, we can use existing techniques for the production and transfer of graphene layers. We constructed an organic film with a graphene layer attached. The fabrication process was as follows. First, ECRIOS (a highly transparent polyimide developed by Mitsui Chemicals, Inc [28].) was dissolved in a solvent, applied to a supporting substrate, and thermally cured at 260°C in N_2. Then, a separately prepared PMMA/graphene stack was transferred onto the ECRIOS film in water. After that, the PMMA was removed with acetone. Finally, the ECRIOS film with the graphene layer was peeled from the supporting substrate. Figure 3(a) shows a fabricated sample. A graphene layer of about 2 cm × 2 cm is attached to a 10-μm thick ECRIOS layer.

The OMPIC consists of a stack of many polymer layers, as described in Section 3. The graphene layer can be formed on a desired polymer layer by applying the graphene transfer to the polymer layer. It can be patterned using O_2 ashing, with an etching mask consisting of an EB resist layer.

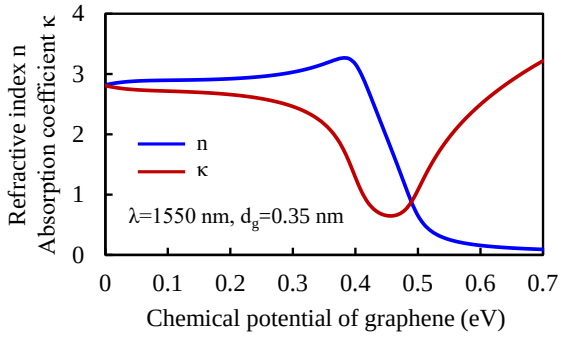

Fig. 2. Refractive index n and extinction coefficient k of graphene as a function of chemical potential, calculated for 1550-nm wavelength.

Optics EXPRESS

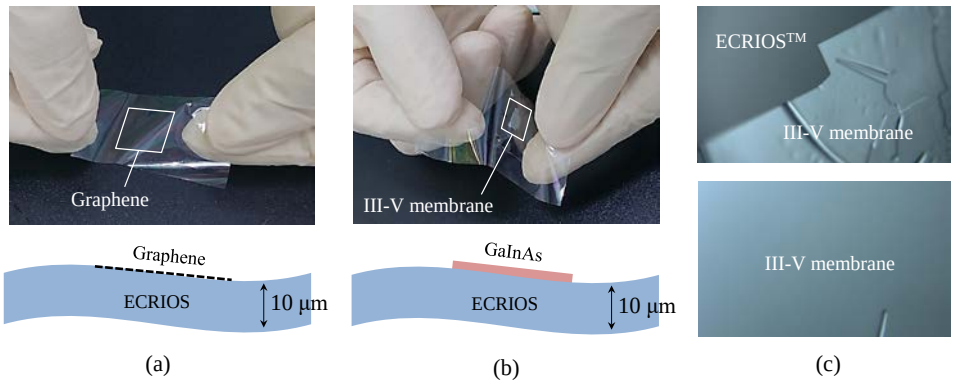

Fig. 3. Fabricated sample of (a) graphene layer and (b) GaInAs layer, each formed on polymer film (on the part surrounded by white frame). (c) Optical micrographs of GaInAs layer near the edge (upper) and away from the edge (lower).

2.2 Thin layer of III-V semiconductor

The second candidate material is a thin semiconductor layer. Most semiconductors, including GaAs, InP, and Si, are bendable to some extent if they are sufficiently thin. For example, the strain limit of InP is about 1% (10^4 ppm), and this corresponds to, for instance, a vertical bending radius of 100 μm for a thickness of 200 nm (which is quite sharp in practice). Although not as flexible as graphene, this is sufficient for practical use in OMPICs. As for electronic functionality, semiconductors are far superior to graphene. In particular, InP is a highly suitable for making photonic devices, and is therefore widely used as a platform material in existing PICs.

In advance of this study, we proposed and developed a method of making InP-based membranes on a Si substrate using benzocyclobutene as a bonding layer [29–31]. This method provides optical waveguides buried in low-refractive-index materials to realize strong light confinement. This enables the construction of small, high-efficiency photonic devices. We have developed this method into a fabrication process for OMPICs.

We made an organic film with a GaInAs layer attached. The fabrication process was as follows. First, a $Ga_{0.47}In_{0.53}As$ layer of 250-nm thickness was formed on an InP substrate with metal–organic chemical vapor deposition. A supporting substrate coated with ECRIOS was then prepared and pretreated at 170°C in N_2. The GaInAs layer with the InP substrate was bonded onto the supporting substrate, followed by thermal curing of the ECRIOS layer at 260°C in N_2. After that, the InP substrate was removed using wet etching. Finally, the ECRIOS film with the GaInAs layer was peeled from the supporting substrate. Figure 3(b) shows a fabricated sample; a thin GaInAs layer is attached to a 10-μm thick ECRIOS layer. The GaInAs layer can be formed without cracks on an organic film (Fig. 3(c) shows optical micrographs of the layer). As in the case of graphene, a semiconductor layer can be formed on a desired polymer layer of OMPICs. The layer can be patterned using CH_4:H_2 dry etching, with an etching mask consisting of an EB resist layer.

3. Method of Fabricating OMPICs

Unlike conventional PICs on conventional rigid platforms, monolithic integration technological barriers of OMPICs including difficulty in achieving the requisite process uniformity and reproducibility have been one of the strongest inhibitors on a manufacturing scale. In addition, monolithically integrating numerous devices and functions inside organic membrane, while at the same time minimizing process complexity, has proven challenging from a design standpoint.

Optics EXPRESS

In this section, we describe a method of fabricating OMPICs, i.e., a technique for integrating various photonic devices monolithically into an organic membrane. Various modifications are possible for the method. The techniques described in this section are simply examples.

3.1 Structure of devices

In advance of the fabrication process, the device structures are briefly explained to highlight the role of each step in the process. The structures are described in detail in Section 4. The device elements integrated in the OMPIC are as follows.

(i) Transmission line (or waveguide)

A transmission line is a simple waveguide composed of a core and some cladding surrounding the core.

(ii) Input/output coupler

In flexible OMPICs, lateral I/O coupling (i.e., input/output from the cross-section of a waveguide) is not easy because of the difficulty of position matching, in addition to the mode size mismatch, between a fiber and the waveguide. Therefore, we adopt vertical coupling (i.e., input/output from the surface of a waveguide) using a metal grating coupler. (See [32] for the grating coupler.)

(iii) Optical path switch

An optical path switch can be made by combining a Mach–Zehnder interferometer or optical ring resonator with a variable phase shifter. For the OMPIC, we use a thermo-optic phase shifter that consists of a waveguide and a metal heater driven by an external current signal.

(iv) Photodetector

A photodetector consists of a waveguide and a layer of electronic material (graphene or semiconductor) placed in proximity to the waveguide. Light in the waveguide generates excess carriers in the electronic material, and this is detected as an electrical signal.

(v) Optical modulator

An optical modulator has almost the same structure as that of the photodetector, but a metal gate is added. The gate voltage changes the carrier density of the electronic material layer and consequently modulates the transmittance of light in the waveguide.

(vi) Laser

It is not practical to integrate a laser in the OMPIC using a thin layer of III-V semiconductors incorporated into an organic membrane, as special measures are needed for heat dissipation. Therefore, lasers are not described in this paper. For practical use, external light sources are suitable for the OMPIC.

3.2 Process flow for fabrication

An example of the fabrication process is illustrated in Fig. 4. Figures 4(a)–4(f) show how each device can be formed. This process uses three thermosetting polymers, namely, ECRIOS (transparent polyimide made by Mitsui Chemicals, Inc.), PMMA (polymethyl methacrylate), and Cytop (amorphous fluoropolymer made by Asahi Glass Co.).

Optics EXPRESS

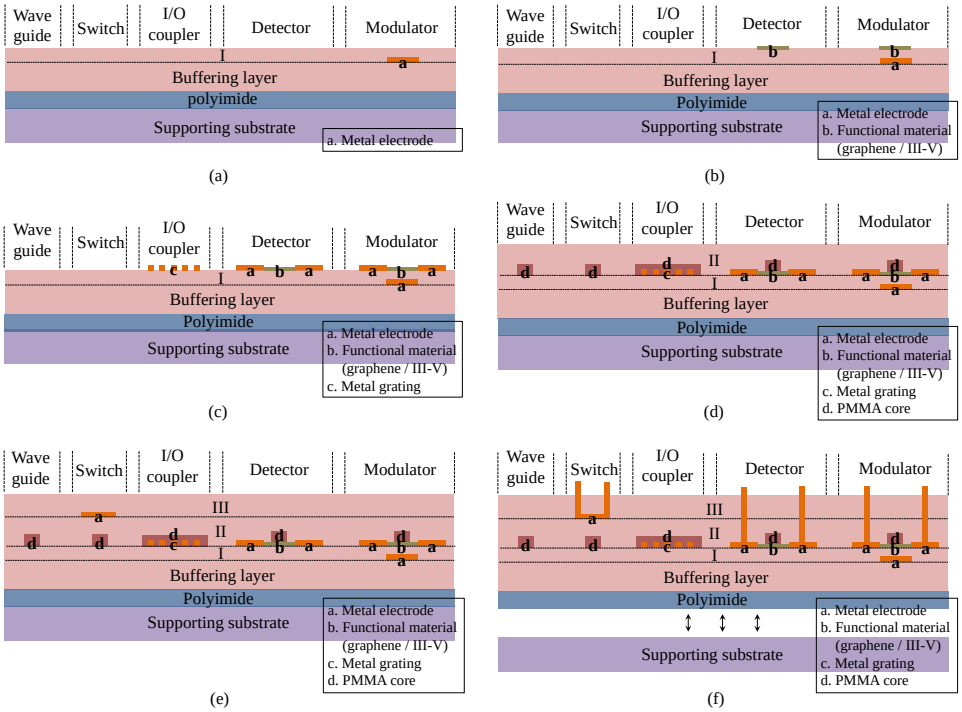

Fig. 4. Process flow to monolithically fabricate OMPICs (one example). Cross section perpendicular to light traveling direction is shown, but only for I/O coupler, cross section in light traveling direction is shown.

- Step 1: Fig. 4(a)

  First, an ECRIOS layer and Cytop layer are formed, in this order, on a supporting substrate (Si, SiO2, InP, etc.). The ECRIOS layer is necessary for peeling the fabricated OMPIC off the substrate in the final stage (step 6) of the process. ECRIOS is a polyimide and therefore easy to peel off; polymers other than polyimide are quite difficult to peel from a substrate. Next, the metal gate of the optical modulator is formed using lithography, metal deposition, and lift-off processing. Then, a Cytop layer (layer I) is formed thereon to make the lower cladding layer of the waveguide.

- Step 2: Fig. 4(b)

  Electronic material layers for the photodetector and the modulator are set on the surface and patterned with lithography and etching. (See Section 2.1 for graphene and Section 2.2 for semiconductor layers.)

- Step 3: Fig. 4(c)

  A metal layer is deposited and patterned to make the electrode of the photodetector and modulator and the metal grating of the I/O coupler.

- Step 4: Fig. 4(d)

  A layer of PMMA is formed on the surface and patterned with electron-beam lithography to form the core of the waveguide. Then, a Cytop layer (layer II) is formed thereon to make the upper cladding layer of the waveguide.

- Step 5: Fig. 4(e)

Optics EXPRESS

A metal layer is deposited and patterned to make the heater for the phase shifter. A Cytop layer (layer III) is then formed; this functions as part of the upper cladding of the waveguide.

- Step 6: Fig. 4(f)

  Contact holes are made through Cytop layers II and III using O_2 plasma etching and filled with metal in order to connect electrodes to the photodetector, modulator, and heater. Finally, the resultant multilayer structure (OMPIC membrane) is peeled from the supporting substrate. This can be done by treating the wafer with an appropriate chemical such as BHF for a surface-oxidized Si substrate and mixed solution $HCl:CH_3COOH$ for an InP substrate. The chemical penetrates between the OMPIC membrane and the substrate and resultantly separates them.

The process flow described above can be modified for each application. One possible modification would be to use ECRIOS alone to make all the polymer layers, except for the waveguide cores, because ECRIOS has high transparency over a wide wavelength range of 400–2000 nm and large tensile strength. In this case, the waveguide core requires the use of a large refractive-index material such as SU-8 (epoxy-based photoresist polymer).

4. Performance limit of OMPIC Devices: Simulation

We theoretically estimated the characteristics of the devices made by the process described in Section 3. Input light was assumed to have a wavelength of 1550 nm. The performance limit calculated for the devices is summarized in Table 1. The following describes the details.

4.1 Transmission line

Figure 5(a) shows the structure of a transmission line (waveguide) along a cross-section perpendicular to the direction of travel of the light. In the simulation, the thickness of the PMMA core was set to 1 μm and both the upper and lower Cytop cladding layers were set to 2 μm. The refractive indices of PMMA and Cytop were assumed to be 1.478 and 1.333, respectively [33, 34].

Table 1. Performance limit of various devices for OMPICs, with graphene as electronic material, calculated for 1550-nm wavelength.

Device	Waveguide	I/O coupler	Switch	PD	Modulator
Core material	PMMA	PMMA	PMMA	PMMA	PMMA
Clad material	Cytop	Cytop	Cytop	Cytop	Cytop
Functional material	-	-	-	Graphene	Graphene
Other features	-	Metal grating	Heat electrode	-	Gate electrode
Calculated characteristics for TE mode	< 0.2dB/bend (R > 100 μm)	7.5dB @Λ = 1140 nm	Δn = 0.6% @2.6 mW on ~0.6 ms off ~1.0 ms	197.5 /cm (μ ~0 eV)	43 → 167 /cm (μ ~0.3 → 0.5 eV)
Calculated characteristics for TM mode	< 0.2dB/bend (R > 100 μm)	7.5dB @Λ = 1100 nm	Δn = 0.6% @2.6 mW on ~0.6 ms off ~1.0 ms	21 /cm (μ ~0 eV)	n/a

Optics EXPRESS

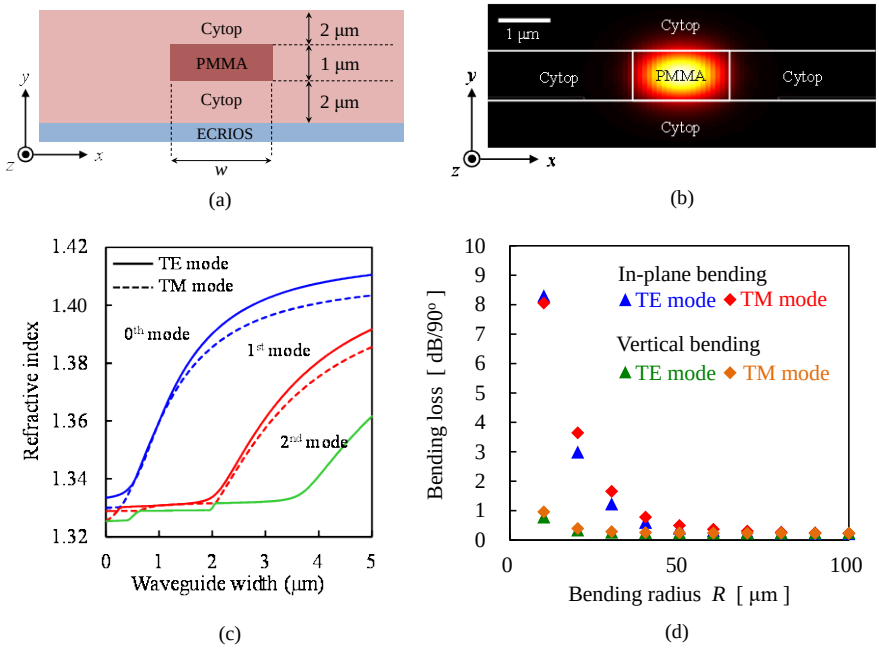

Fig. 5. Transmission line (waveguide). (a) Device structure and (b) optical field distribution, cross section perpendicular to light traveling direction; (c) calculated equivalent refractive index of several low-order modes as a function of the width of the waveguide; (d) in-plane and vertical bending loss at 90° bending as a function bending radius *R*.

We simulated the propagation of light in the waveguide using the finite element method (FEM). One example of the optical field distribution is visualized in Fig. 5(b). Figure 5(c) depicts the calculated equivalent refractive index as a function of the waveguide width for low-order modes. From this result, single-mode propagation can be realized with a core width of 2 μm for both TE and TM modes. We analyzed the bending loss of the waveguide with the 2-μm wide core using the finite-difference time-domain (FDTD) method. Figure 5(d) shows the calculated in-plane and vertical bending loss at 90° bending as a function of the bending radius. For both TE and TM modes, in-plane bending loss (i.e., bending inside optical circuits) is 0.2 dB or lower for a bend radius of 100 μm, and vertical bending loss (i.e., physical bending of the film) is lower than 0.2 dB for a 30-μm bend radius.

4.2 I/O coupler

Figure 6(a) shows the I/O coupler along a cross-section in the direction of travel of the light. To obtain a highly efficient coupling, we used a thin metal grating buried in the PMMA core of the waveguide, which can easily be fabricated using standard processes. The coupler is connected to a transmission line through a tapered waveguide to realize single-mode propagation (see the planar pattern given below).

We simulated the propagation of light to calculate the coupling efficiency using FDTD. In the simulation, the grating was assumed to be Au-Ti double layer stripes (30-nm thick Au (upper) plus 10-nm thick Ti (lower)) arrayed with a duty ratio of 50% and 30 cycles. To attain a high coupling efficiency, the width of the grating and the PMMA core of the coupler was set to 30 μm, a far larger than the transmission line width. Input light beam (collimated with a ball-lensed fiber) with a 10-μm diameter was applied to the coupler from 7 μm above the Cytop surface. The incident angle θ of the input light was set to 1°.

Optics EXPRESS

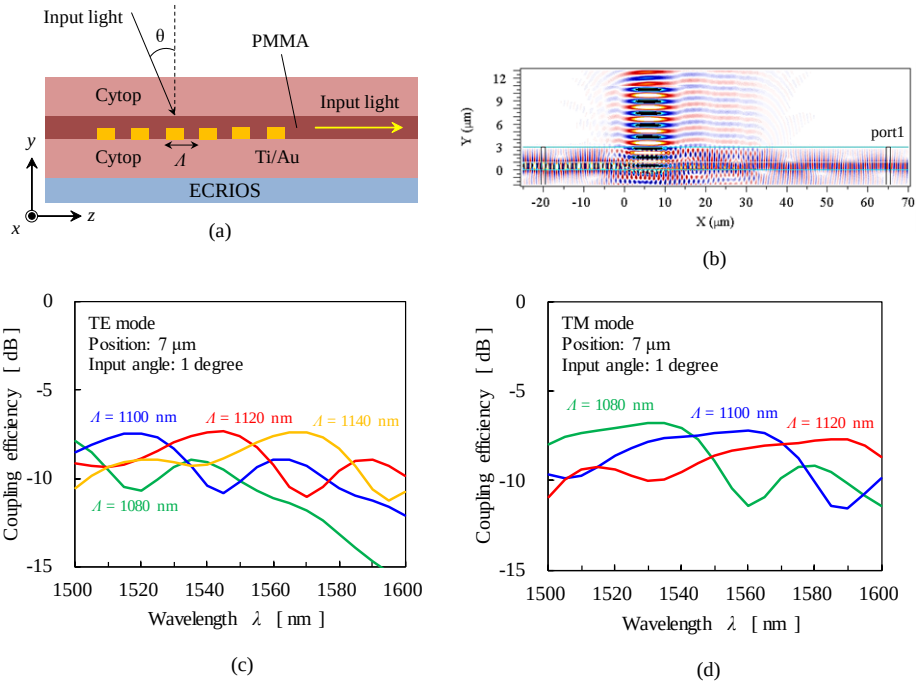

Fig. 6. I/O coupler. (a) Device structure and (b) optical field distribution, cross section in light traveling direction; (c) TE-mode and (d) TM-mode coupling efficiencies as a function of wavelength λ, with grating pitch Λ as a parameter.

Figure 6(b) visualizes one example of the optical field distribution, showing how light incident on the grating propagates to the waveguide. We calculated the coupling efficiency of the coupler by taking the power ratio of output light at port 1 and incident light in Fig. 6(b). Figures 6(c)–6(d) show the coupling efficiencies for TE and TM modes, calculated as a function of wavelength, with the grating pitch parameter Λ. For the TE mode, the efficiency at 1545-nm wavelength reaches the maximum of −7.5 dB with a grating pitch of 1120 nm. In TM mode, a wavelength of 1560 nm gives the maximum efficiency of −7.5 dB with a grating pitch of 1100 nm. (Light after passing through the grating included multiple modes slightly. This is due to the large width of the grating and the PMMA core. However, the multiple mode component can be removed by leading the light to a transmission line through a tapered waveguide.)

4.3 Phase shifter for optical path switch

Figure 7(a) shows the thermo-optic phase shifter for optical path switches along a cross-section perpendicular to the direction of light travelling. The device consists of a waveguide and a metal heater placed above the waveguide. The heater is made of the Au-Ti double layer and driven by an external current signal to change the temperature of the waveguide. A large temperature rise can be obtained with little electric power because the device is surrounded by polymers with low thermal conductivity.

Using a two-dimensional model implemented with FEM, we calculated the distribution of temperature when a current is applied to the heater and, using the result, calculated a change in the refractive index of the waveguide at 1550-nm wavelength. The simulation was based on the typical heat transfer equation

Optics EXPRESS

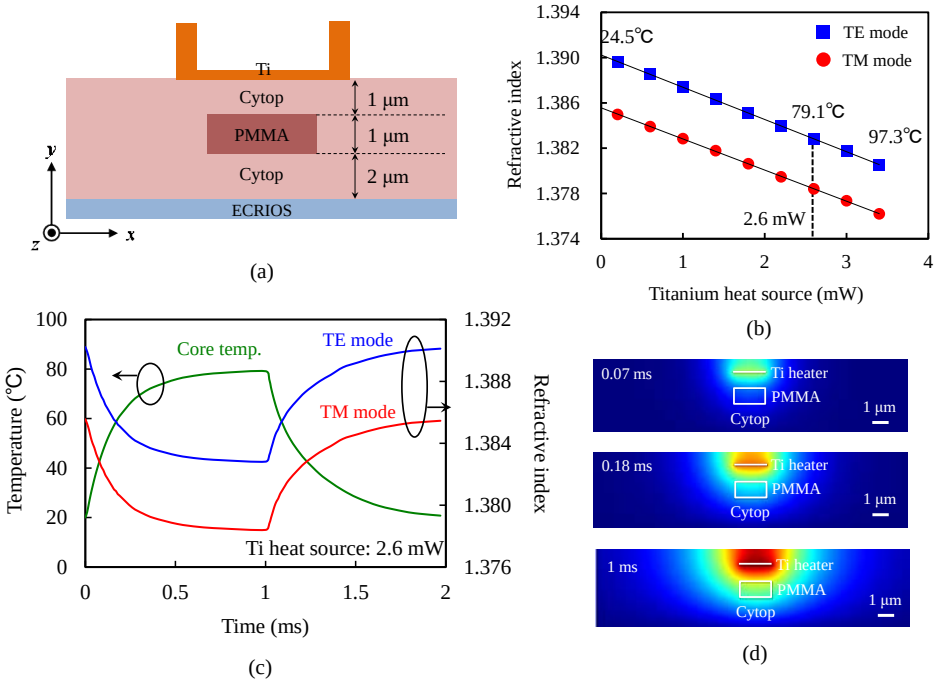

Fig. 7. Phase shifter. (a) Device structure, cross section perpendicular to light traveling direction; (b) refractive index of the waveguide modes as a function of heater power dissipation. Temperature at the center of the core is written in the figure; (c) time-dependent refractive index change with 2.6-mW heater power; (d) temperature distribution at each instant of time.

$$\rho C \frac{\partial T}{\partial t} - \nabla \cdot (\kappa \nabla T) = Q \tag{3}$$

where Q is the heat source density, T is temperature, κ is the thermal conductivity, ρ is the heat density, and C is the specific heat capacity. In the simulation, κ, ρ, and C were set to 0.21 W/m·K, 1190 kg/m^3, and 1300 J/kg·K for PMMA and 0.12 W/m·K, 2030 kg/m^3, and 1500 J/kg·K for Cytop [33, 34]. Figure 7(b) shows the calculated refractive index of the phase shifter as a function of heater power dissipation. A change of ~0.6% can be obtained with 2.6-mW heater power in both TE and TM modes. Figure 7(c) depicts the time-dependent refractive index change with 2.6-mW heater power; the temperature distribution at each time is visualized in Fig. 7(d). The time constant of operation was ~0.6 ms at heater-on and ~1 ms at heater-off. Using this element, a phase of light in a Mach–Zehnder interferometer and optical ring resonator can be controlled with an external current signal to achieve optical path switching.

This element can also be used as a temperature sensor. For this purpose, the heater is not needed; rather, a thermo-induced phase shift in the waveguide is employed. In combination with a Mach–Zehnder interferometer or optical ring resonator, this device can operate as a highly sensitive temperature sensor.

4.4 Photodetector

We used graphene as the electronic material for a photodetector because, compared with ultra-thin semiconductor layers, it has a large light absorption efficiency and small carrier relaxation time. Figure 8(a) shows the structure of the photodetector along a cross-section perpendicular to the direction of travel of the light. The device consists of a waveguide and a

Optics EXPRESS

graphene layer placed immediately under the PMMA core of the waveguide. Electrodes are attached to both ends of the graphene layer. Light in the waveguide generates excess carriers in the graphene layer, and this is detected as an electric signal through the electrodes.

We performed mode analysis on this structure with the aid of FEM, using the optical properties (Section 2.1) of graphene. The graphene layer was assumed to be an anisotropic medium with a thickness of 0.35 nm. Figure 8(b) visualizes one example of the TE-mode optical field distribution. Figure 8(c) depicts the effective refractive index and light absorption coefficient of the detector as a function of the chemical potential of graphene, calculated for both 1550-nm TE and TM modes. To achieve efficient light absorption, the chemical potential should be set to nearly 0 eV for both TE and TM modes. Subsequently, absorption coefficients of 197.5 cm^{-1} (TE mode) and 21 cm^{-1} (TM mode) were obtained. This means that light absorption of 90% can be obtained with a device length of about 115 μm for TE mode—sufficient for the practical use of OMPICs. In contrast, a device length required for TM-mode light absorption of 90% reaches 1 mm.

Finally, we calculated the wavelength dependence of the effective refractive index and light absorption coefficient of the detector. The chemical potential of graphene was assumed to be nearly 0 eV for both TE and TM modes. Figure 8(d) shows the results. For wavelengths of 1300–1700 nm, the absorption coefficient for the TE mode is 166-240 cm^{-1}, weakly dependent on the wavelength.

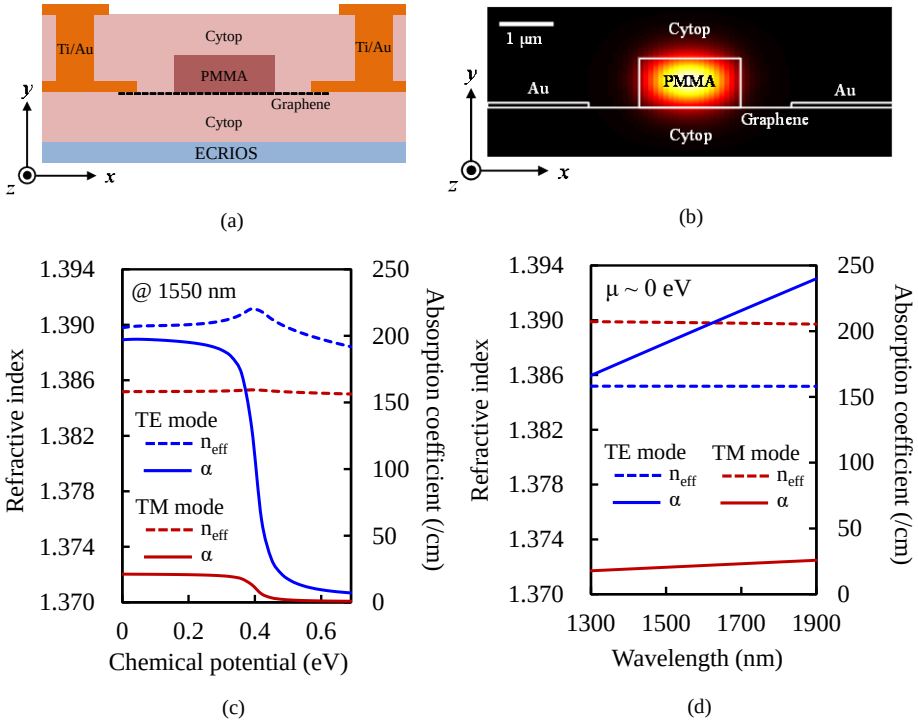

Fig. 8. Photodetector. (a) Device structure and (b) TE-mode optical field distribution, cross section perpendicular to light traveling direction; (c) effective refractive index n_{eff} (dashed line) and light absorption coefficient α (solid line) as a function of chemical potential of graphene layer, calculated for 1550-nm wavelength; (d) wavelength dependence of refractive index (dashed lines) and absorption coefficient (solid lines).

4.5 Modulator

We also used graphene for the optical modulator. Figure 9(a) shows the structure of the modulator along a cross-section perpendicular to the direction of light travelling. The device

Optics EXPRESS

has almost the same structure as that of the photodetector, with the addition of a gate under the graphene layer with a 500-nm-thick Cytop layer in between. The gate voltage changes the chemical potential (and therefore the carrier density) of the graphene, causing the graphene to switch from dielectric-like to metallic. This allows the transmittance of light in the waveguide to be modulated by the gate voltage. Among organic polymers, Cytop has a large dielectric strength and can therefore be used as a gate insulator as well as a cladding layer.

We conducted mode analysis on this structure using FEM. The graphene layer was assumed to be an anisotropic medium with a thickness of 0.35 nm. Figure 9(b) visualizes one example of the TE-mode optical field distribution. Figure 9(c) depicts the effective refractive index and light absorption coefficient of the modulator as a function of the chemical potential of the graphene for a wavelength of 1550 nm. Compared with the results for TE mode, light absorption for TM mode is extremely large due to a plasmon excitation of the gate under the graphene layer. Therefore, TM-mode light is not suitable for modulators in OMPICs. For efficient modulation with a small gate-voltage swing, the graphene chemical potential should be biased to about 0.3-0.5 eV for TE mode. In this condition, the absorption coefficient can easily be switched between 43 cm^{-1} and 167 cm^{-1} for TE mode (i.e., optical attenuation between −2.6 dB and −10 dB in a 140-μm long device).

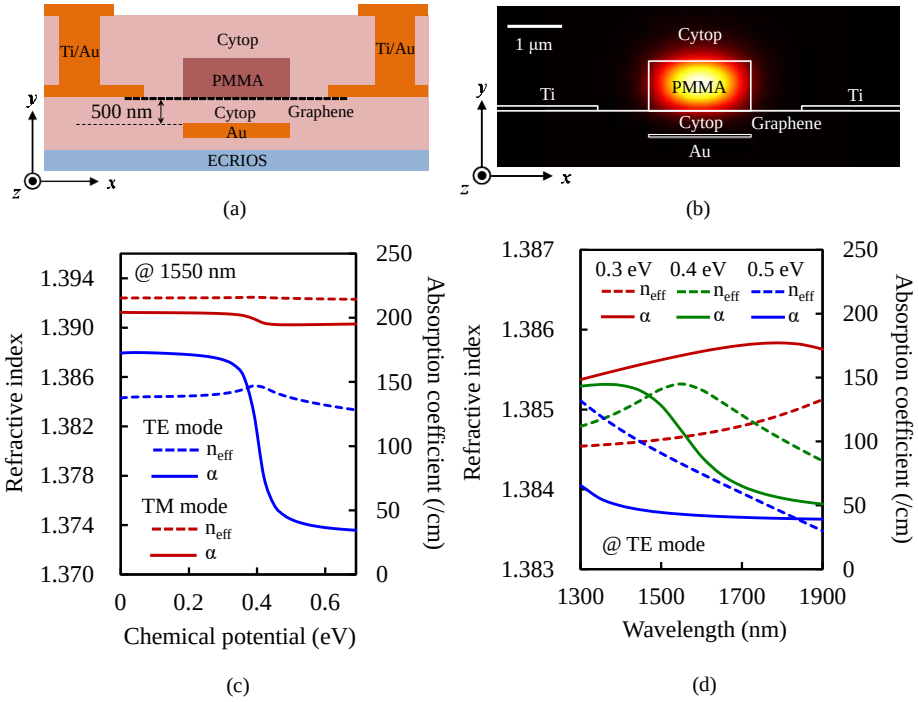

Fig. 9. Optical modulator. (a) Device structure and (b) TE-mode optical field distribution, cross section perpendicular to light traveling direction; (c) effective refractive index n_{eff} (dashed line) and light absorption coefficient α (solid line) as a function of chemical potential of graphene layer, calculated for 1550-nm wavelength; (d) wavelength dependence of refractive index (dashed lines) and absorption coefficient (solid lines) for TE-mode light, with graphene chemical potential μ as a parameter.

We also calculated the wavelength dependence of the refractive index and absorption coefficient for TE mode. Figure 9(d) show the results. In Fig. 9(d), the increase in chemical potential causes the sharp change in the absorption coefficient to move to lower wavelengths, which has a direct influence on absorption modulation. For a chemical potential of around 0.4 eV, a large change in the TE-mode absorption coefficient occurs at broadband wavelengths of 1300–1900 nm.

Optics EXPRESS

5. Making and Measuring Actual Devices: Transmission Lines and I/O Couplers

As the first step in actual device fabrication, we monolithically integrated a transmission line and I/O couplers, the most basic elements of the OMPIC, in an organic membrane. Figure 10(a) shows the appearance of the fabricated device. The transmission line and I/O couplers are integrated in a transparent membrane with a thickness of about 10 μm. The planar pattern of the fabricated device is illustrated in Fig. 10(b); the couplers are connected to both ends of the transmission line through tapered waveguides (Fig. 10(b) also shows a photomicrograph of the right half of the device).

The fabrication process was as follows. An InP wafer was used as a supporting substrate (although other materials could also be used). First, ECRIOS and Cytop layers of 2 μm were coated, in this order, onto the substrate and thermally cured. A photoresist pattern for the gratings was then formed on the surface using electron-beam lithography; a 10-nm Ti layer and 30-nm Au layer were deposited thereon, in this order; this Ti-Au double layer was patterned into the gratings for the I/O couplers using lift-off processing. After that, PMMA was coated thereon and patterned to make the core of the waveguides; the thickness and width of the PMMA core were set to be 1 μm and 2 μm, respectively. A Cytop layer of 2 μm was again formed on the surface for passivation. Finally, the resultant multilayer film (OMPIC membrane) was peeled from the supporting substrate by treating the wafer with mixed solution HCl:CH_3COOH.

We measured the transmission of light in the device with waveguide lengths of 2–8 mm. The TE-polarized light from an external wavelength-tunable laser was coupled into the metal grating by using a ball-lensed single-mode fiber. Figure 10(c) shows the results for a wavelength of 1550 nm. From this, we calculated the propagation loss of the transmission line and the coupling loss of the coupler (metal grating and tapered waveguide) to be 1.4 dB/cm and 27 dB/coupler, respectively. Although the coupling loss is relatively large, it can probably be lowered toward the theoretical expectation of 7.5 dB/coupler by improving the fabrication process and optimizing the structure of the grating. The low coupling efficiency results from that we used the same temperature (110°C in this experiment) to cure the first and second Cytop layers. The 110°C treatment for the second Cytop softened the cured first Cytop layer slightly, and this distorted the metal grating formed on the first Cytop to reduce the coupling efficiencty. This can be avoided by using a slightly higher temperature to cure the first Cytop layer [35]. With this, a high coupling efficiency close to the theoretical value can be achieved.

Figure 10(d) plots the intensity of the measured output light for the experimental device with waveguide lengths of 8 mm, as a function of wavelength from 1524 to 1575 nm. A large wavelength dependence occurred for the same reason mentioned above. Improving fabrication process will enable to make the transmission intensity almost constant in this wavelength range.

Optics EXPRESS

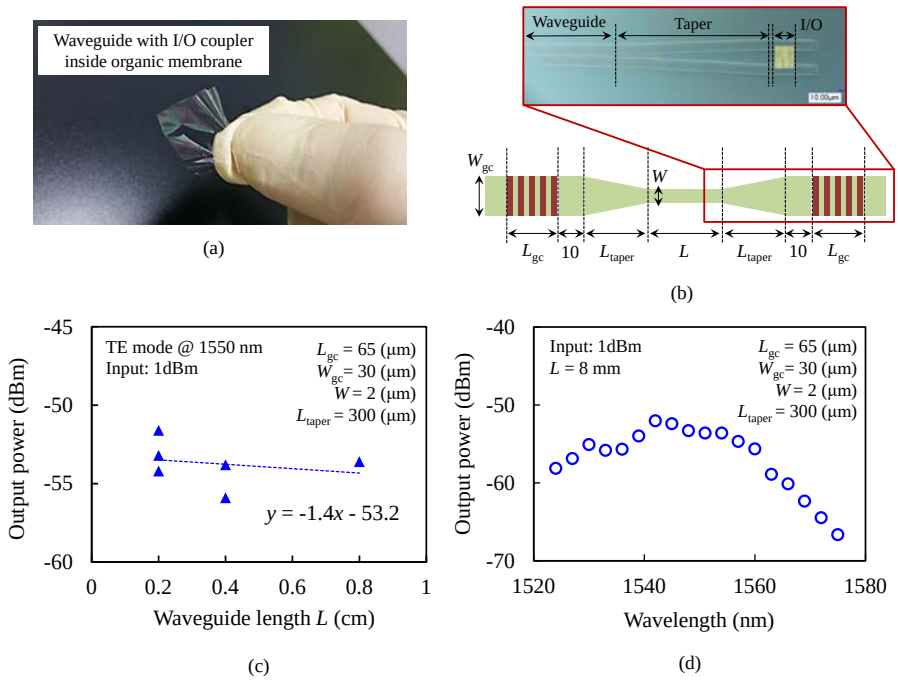

Fig. 10. Prototype of transmission line and I/O couplers. (a) Devices integrated into organic membrane; (b) photomicrograph of right half of devices; (c) transmission characteristic as a function of transmission line length L, measured for 1550-nm wavelength. Planar pattern of devices is also shown; (d) intensity of the measured output light for the experimental device with waveguide lengths of 8 mm, plotted as a function of wavelength.

6. Summary

The orthodox application of photonic integrated circuits is in the field of high-speed, large-capacity internet systems. However, photonic integrated circuits are expected to have many other applications that make use of optical functionalities. As a first step toward such new application fields, we have proposed the concept of OMPICs (organic membrane photonic integrated circuits), which incorporate various functions needed for optical signal processing into organic membranes of several microns in thickness. In this paper, we described the structure of several photonic devices for OMPICs and estimated the characteristics of these devices using computer simulations. We then presented a method of fabricating the photonic devices monolithically in an organic membrane and, as a first step, demonstrated the operation of a transmission line and I/O couplers, the most basic elements of OMPICs. One direction for further developments in OMPICs would be their combination with organic field-effect transistor (OFET) circuits, which have enjoyed rapid progress in recent years. It appears that OFET circuits are compatible with OMPICs in terms of both their geometry and fabrication process. The combination of photonic functionality in OMPICs with the electronic functionality of OFETs can be expected to open up innovative fields of photonics and electronics.

Funding

JST CREST Grant Number JPMJCR15N6 and JSPS KAKENHI Grant Numbers 15H05763, 16H06082, 14J02327, and 16J11581.